BIOMEDICAL ENGINEERING

10.1126/sciadv.1501478

Biodegradable triboelectric nanogenerator as a life-time designed implantable power source

Qiang Zheng,[1] Yang Zou,[2] Yalan Zhang,[2] Zhuo Liu,[2] Bojing Shi,[1] Xinxin Wang,[1] Yiming Jin,[1] Han Ouyang,[1] Zhou Li,[1]* Zhong Lin Wang[1,3]*

Transient electronics built with degradable organic and inorganic materials is an emerging area and has shown great potential for in vivo sensors and therapeutic devices. However, most of these devices require external power sources to function, which may limit their applications for in vivo cases. We report a biodegradable triboelectric nanogenerator (BD-TENG) for in vivo biomechanical energy harvesting, which can be degraded and resorbed in an animal body after completing its work cycle without any adverse long-term effects. Tunable electrical output capabilities and degradation features were achieved by fabricated BD-TENG using different materials. When applying BD-TENG to power two complementary micrograting electrodes, a DC-pulsed electrical field was generated, and the nerve cell growth was successfully orientated, showing its feasibility for neuron-repairing process. Our work demonstrates the potential of BD-TENG as a power source for transient medical devices.

INTRODUCTION

Electronics used for implantable medical devices have some specific requirements that are more restrictive than for other applications, such as high reliability, long lifetime, biocompatibility, and/or biodegradability (*1*–*3*). In this context, electronic systems entirely built with biodegradable materials are of growing interest for their potential applications in systems that can be integrated with living tissue and used for diagnostic and/or therapeutic purposes during certain physiological processes (*4*–*9*). The devices can be degraded and resorbed in the body, so no operation is needed to remove them and adverse long-term side effects are avoided. A great deal of work has been done studying those degradable transient electronics built with absorbable organic and inorganic materials for in vivo sensors and therapeutic devices (*10*–*17*). However, most of these devices need external power sources for operation, which may limit their applications for in vivo cases (*18*).

Here, we reported a biodegradable triboelectric nanogenerator (BD-TENG) for short-term in vivo biomechanical energy conversion. Enabled by the design of a multilayer structure that is composed of biodegradable polymers (BDPs) and resorbable metals, the BD-TENG can be degraded and resorbed in an animal body after completing its work cycle without any adverse long-term effects. Tunable electrical output capabilities and degradation features were achieved by fabricated BD-TENG with different materials. The open-circuit voltage (V_{oc}) of BD-TENG can reach up to ~40 V, and the corresponding short-circuit current (I_{sc}) was ~1 μA. When applying BD-TENG to power two complementary micrograting electrodes, a DC-pulsed electric field (EF) was generated (1 Hz, 10 V/mm), and the nerve cell growth was successfully orientated, which was crucial for neural repair. Our work demonstrated the potential of BD-TENG as a power source for transient implantable medical devices.

[1]Beijing Institute of Nanoenergy and Nanosystems, Chinese Academy of Sciences, National Center for Nanoscience and Technology (NCNST), Beijing 100083, PR China. [2]School of Biological Science and Medical Engineering, Beihang University, Beijing 100191, PR China. [3]School of Materials Science and Engineering, Georgia Institute of Technology, Atlanta, GA 30332–0245, USA.
*Corresponding author. E-mail: zlwang@binn.cas.cn (Z.L.W.); zli@binn.cas.cn (Z.L.)

RESULTS

The BD-TENG was fabricated mostly using BDPs (*19*, *20*). From a biomaterial point of view, the materials selected for BD-TENG should be biodegradable, have excellent biocompatibility, be compatible with a variety of polymer processing, and have been previously used in biomedical devices. Furthermore, when used as the friction part of the TENG, the polymers should exhibit a different tendency to gain and lose electrons (*21*). These constraints on material properties led to the selection of poly(L-lactide-*co*-glycolide) (PLGA), poly(3-hydroxybutyric acid-*co*-3-hydroxyvaleric acid) (PHB/V), poly(caprolactone) (PCL), and poly(vinyl alcohol) (PVA) to be used in fabricating BD-TENG. All of these polymers are low-cost, commercially available, and soluble in suitable solvent systems to promote facile processing methods, including casting and spin coating.

The as-fabricated BD-TENG has a multilayered structure: the encapsulation structure, the friction layers, the electrode layers, and the spacer, as sketched in Fig. 1. Two of the selected BDP layers (PLGA, PVA, PCL, and PHB/V) with patterned nanoscale surface structures were assembled together as friction parts (Fig. 1, A and B), and a spacer (200 μm) composed of BDP was set between these friction layers to effectively separate them. A thin magnesium (Mg) film (50 nm) was deposited on one side of each friction layer as an electrode layer. The whole structure was encapsulated in BDP (100 μm) to keep it from contacting the surrounding physiological environment (Fig. 1, C and D).

As a demonstration of the biocompatibility of the constituent materials, we cultured endotheliocytes (ECs) with the as-synthesized BDP films (~100 μm). Most ECs were viable after 7 days of culture and showed no difference with a control group (standard cell culture dish). Moreover, intact cytoskeletal structures were also detected, suggesting that most of the ECs were healthy (Fig. 1G).

The electricity-generating process relies on the relative contact separation between two BDP friction layers, in which a unique coupling between triboelectrification and electrostatic induction gives rise to an alternating flow of electrons between electrodes. This process is described as the vertical contact separation mode of TENG (*22*–*27*) (Fig. 2A). When an external force brings those two friction

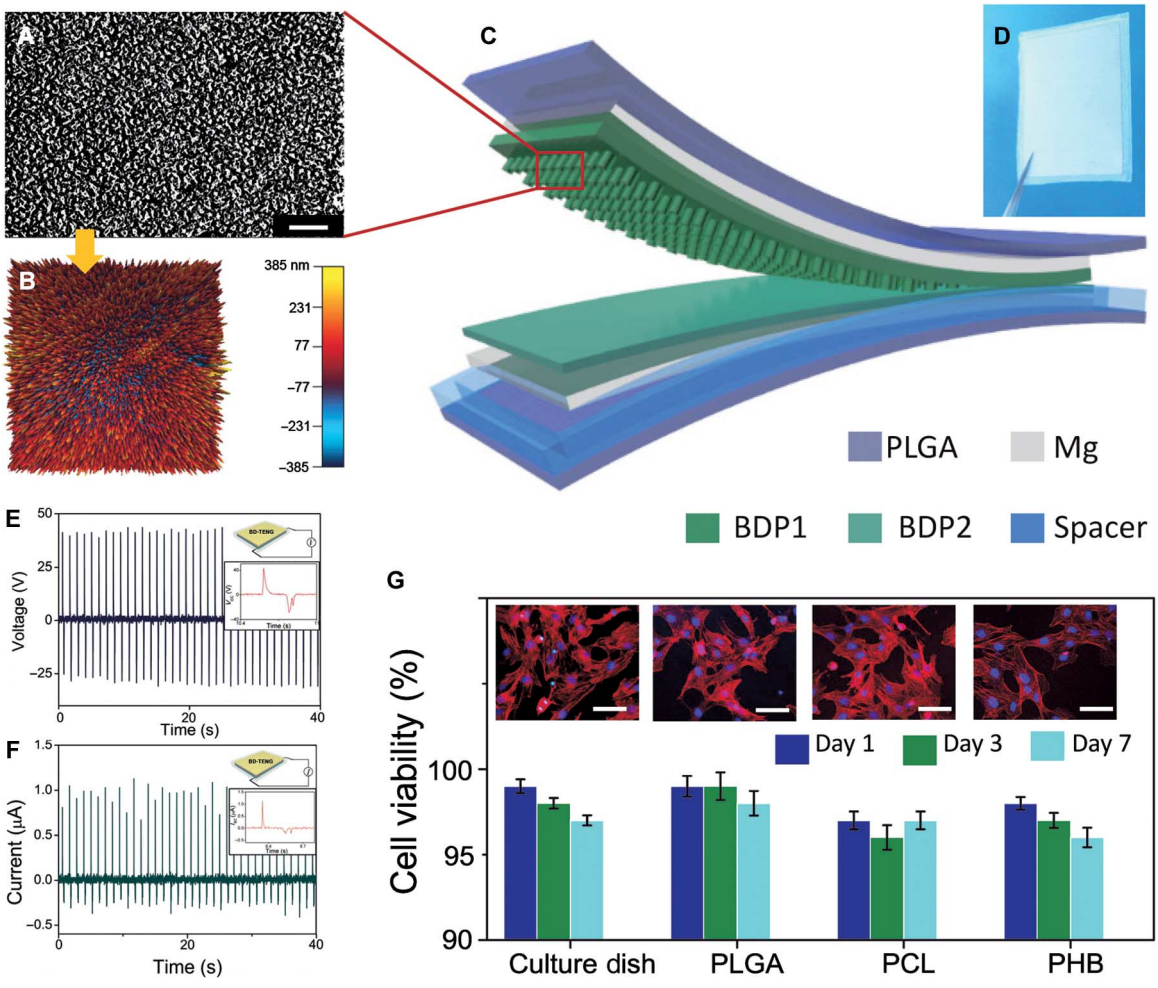

Fig. 1. Device structure, typical output performance, and cytocompatibility of BD-TENG. (**A** and **B**) SEM and atomic force microscopy (AFM) images of the nanostructure on the BDP film (scale bar, 10 μm). (**C** and **D**) Schematic diagram and photograph of BD-TENG. (**E** and **F**) Measured electrical signals by applying an external force: (E) V_{oc} and (F) I_{sc}. (**G**) Cell viability after cells were cultured with different BDP films for 7 days. (Inset: Fluorescence images of stained endothelial cells that were cultured on BDP films. Scale bar, 100 μm.)

layers (PLGA/PCL) into contact, electrons are transferred from PLGA to PCL and retained on both BDPs, resulting in surface triboelectric charges. The subsequent release of the external force caused the separation of PLGA from PCL films, formed an electrical potential between those two films that drives the electrons through external loads, and screened the inductive charges on both magnesium electrodes. As the periodically applied external force keeps affecting the BD-TENG, AC electrical pulses are generated.

To test the in vitro output performance of the BD-TENG, we used a mechanical linear motor to apply impulse impact. The frequency was set at 1 Hz for simulating low-frequency biomechanical motion. The V_{oc} could reach up to ~40 V, and the I_{sc} could be as high as ~1 μA (Fig. 1, E and F). Resistors were connected as external loads to further investigate the effective electric power of the BD-TENG. As demonstrated in fig. S2, the instantaneous current drops with increasing load resistance because of ohmic loss, whereas the voltage builds up. Consequently, at a load resistance of 80 megohms, a power density of 32.6 mW/m^2 for BD-TENG was achieved (fig. S2, E and F).

The intrinsic electrical properties of two friction layers significantly affect the output performance of TENG, for example, the ability of gaining or losing electrons. For some materials, this ability has been tested and ranked in terms of "triboelectric series" (*20*, *28*). Because the selected BDPs (PLGA, PCL, PHB/V, and PVA) have diversified molecular structures and functional groups, we assumed that their triboelectrical properties are of difference. Therefore, we designed a classical TENG system to test their relative ability of gaining or losing electrons in a triboelectric process. Typically, a Kapton film was applied as the reference contact layer of TENG. The transferred charges between the BDP friction layer and Kapton were recorded. In reference to the relative ability to gain or lose electrons, we ranked this relatively electrical property as the "BDP triboelectric series," in which the charge tendency of the selected BDPs in a triboelectrification process was demonstrated as PLGA > PHV/B > PVA > PCL from positive to negative (Fig. 2B). Under the guidance of this BDP triboelectric series, we fabricated BD-TENG using a different combination of BDPs, and different electric output was generated for their different triboelectrical properties. Here, the in vitro

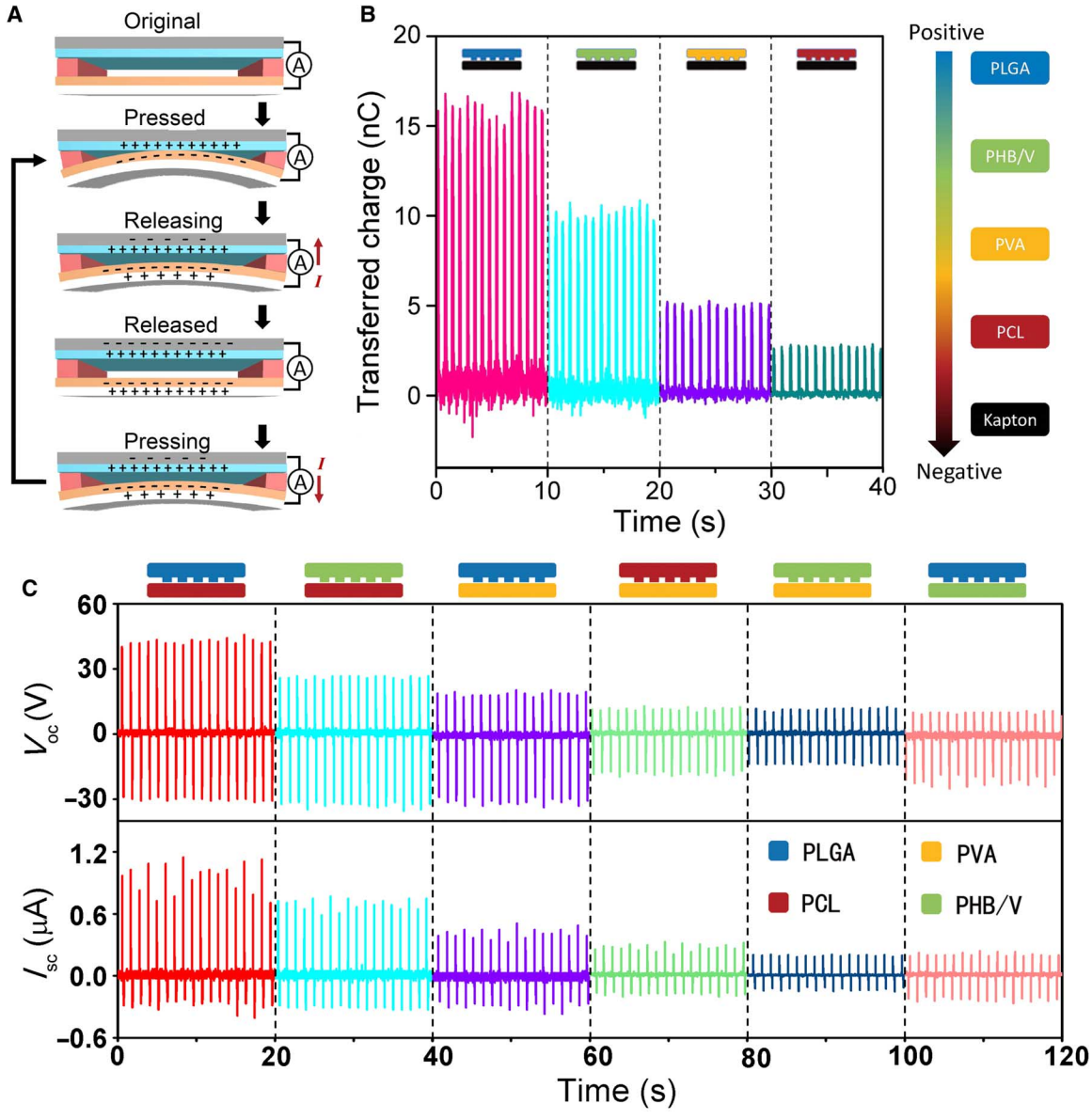

Fig. 2. The working principle and electrical output modulating of BD-TENG by changing the materials of friction layers. (**A**) Schematic diagram of the working principle of BD-TENG. (**B**) Relative ability to gain or lose electrons of the selected BDPs. All candidate materials were coupled with Kapton film, and the transferred charges were recorded as the sign of the relative ability to gain or lose electrons. (**C**) Output performance of BD-TENG with different friction layers. Top: V_{oc}. Bottom: I_{sc}.

output performance of BD-TENG (size, 2.0 × 3.0 cm) could be tuned in a large range from ~10 to ~40 V just by modulating the composition materials (Fig. 2, C and D).

The surface topology structure is important for the output performance of TENG (*29*–*31*). We developed an etching method for fabricating surface nanostructures of BDP films. The reaction conditions should be carefully controlled, avoiding obvious destruction of the whole structure. BDP films were incubated with 2 M NaOH solution at 40°C. By carefully controlling the incubation time, uniform nanorod arrays could be formed on the surface. Taking PLGA as an example, the height of a nanoarray could be up to 300 nm within 10 min of etching (Fig. 3A). The PLGA films (2 × 3 cm) with different surface nanostructures (etching time: 0, 5, and 10 min) were coupled with the same PVA film to test the output under the drive of a liner motor. As the etching time increased, the surface nanostructure gradually appeared, and the corresponding V_{oc} was increased from 16 to 32 V (Fig. 3B).

In vitro biodegradation studies were performed to investigate device absorption characteristics. It is widely accepted that hydrolytic degradation of the BDP films can proceed via surface and bulk degradation pathways (*32*–*35*), as depicted schematically in fig. S2A. In most cases, the BDP first goes through a long period that appears stable and unchanged, then degrades quickly. The whole structure "vanishes" in a relatively short period of time. Here, we exposed BD-TENGs with

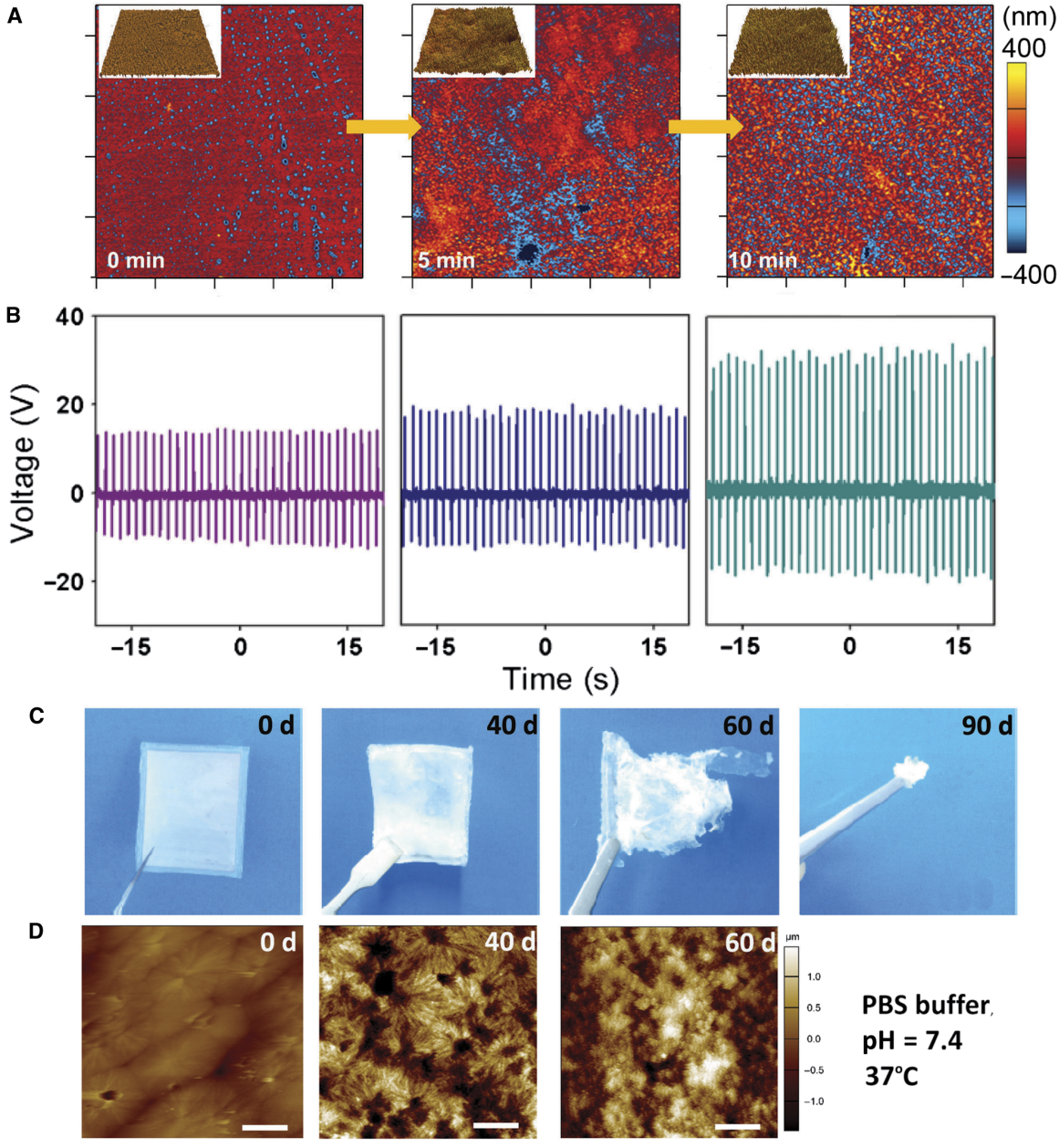

Fig. 3. Output of BD-TENG related to different surface morphologies and in vitro degradation process of device. (**A**) AFM image of PLGA film incubated with NaOH for different times. (**B**) Electrical output signals of FDNG with differently patterned PLGA film. (**C**) Photographs from BD-TENG at various stages of the degradation time line suggest that devices encapsulated in PLGA were initially resistant to mass degradation. However, after 40 days, significant mass loss and structure disintegration was initiated. Near-total mass loss was observed at 90 days. (**D**) AFM image from the surface of BD-TENG at different degradation times demonstrates the destruction of the BDP structure throughout the degradation process (scale bar, 20 μm).

different encapsulation materials to PBS (phosphate-buffered saline) buffer (pH 7.4) at 37°C. Irreversible loss of functionality was found at different time intervals as the encapsulation layer gradually swelled and water infiltrated into the inner structure of the BD-TENG. The PLGA (75:25)–encapsulated device was relatively resistant to mass loss and water uptake at the initial stage (0 to 30 days), and only slight hydrolytic cleavage of the polymer backbone happened at the surface. As the BD-TENG began to undergo rapid autocatalytic hydrolysis and bulk degradation, a marked mass loss and surface erosion took place (Fig. 3, C and D). Once the water leaked into the inner structure of the BD-TENG, the Mg electrode dissolved within 24 hours (fig. S2C). Structural integrity was lost at ~50 days, at which point the encapsulation layer was hydrolyzed into a viscous gel composed of low-molecular-weight PLGA. The mass loss progression of other BDP encapsulation layers was also evaluated in PBS buffer at 37°C for 3 months (fig. S2B) and was consistent with previous reports (*36*–*38*). The efficient in vivo working time of BD-TENG could be designed according to the different degradation times of BDPs. This

is crucial for powering temporal implantable medical devices with different lifetimes.

A fundamental understanding of the in vivo degradation phenomenon as well as the evaluation of cellular and tissue responses plays a key role in the design and development of biodegradable devices for therapeutic application. To demonstrate their potential for in vivo applications, we conducted a series of experiments for evaluating BD-TENGs with short-time or long-time degradation properties. Two representative BD-TENGs were fabricated and sealed in PVA and PLGA encapsulation, respectively. Those devices were sterilized by γ irradiation (^{60}Co/25 kGy) and then implanted in the subdermal region of SD rats (Fig. 4, A and E), the procedure strictly following the "Beijing Administration Rule of Laboratory Animals" and the national standard "Laboratory Animal Requirements of Environment and Housing Facilities (GB 14925-2001)." Figure 4A shows the case of the PLGA-coated BD-TENG. After 9 weeks of implantation, the wound healed well, and no obvious infection was detected, revealing good biocompatibility of BD-TENGs (Fig. 4B). The histological section showed the site where the BD-TENG was located between the subdermal layer and the muscle layer and surrounded by a small amount of fibrous tissue (Fig. 4F). No significant inflammatory reaction was detected, as required for implantation of devices. Tissue fluid was also extracted from the implant site at different time intervals. Few neutrophilic granulocytes were observed before week 4, although the number was not increased obviously over time, revealing good biocompatibility of BD-TENGs (fig. S4).

The output performance of BD-TENGs was monitored throughout the implantation process (Fig. 4G). As for PLGA-coated BD-TENGs, the voltage was markedly decreased from 4 to 1 V after 2 weeks of implantation. This could be attributed to the restriction of a fibrous capsule surrounding the BD-TENG and the swelling of the encapsulation layer (Fig. 4G). Although no water infiltrated into the inner gap between the friction layers, the deformed outer layer would significantly restrict the contact, releasing the motion of BD-TENG and subsequently affecting the output performance. The electrode wires that were fixed on the Mg electrodes fell off at week 4,

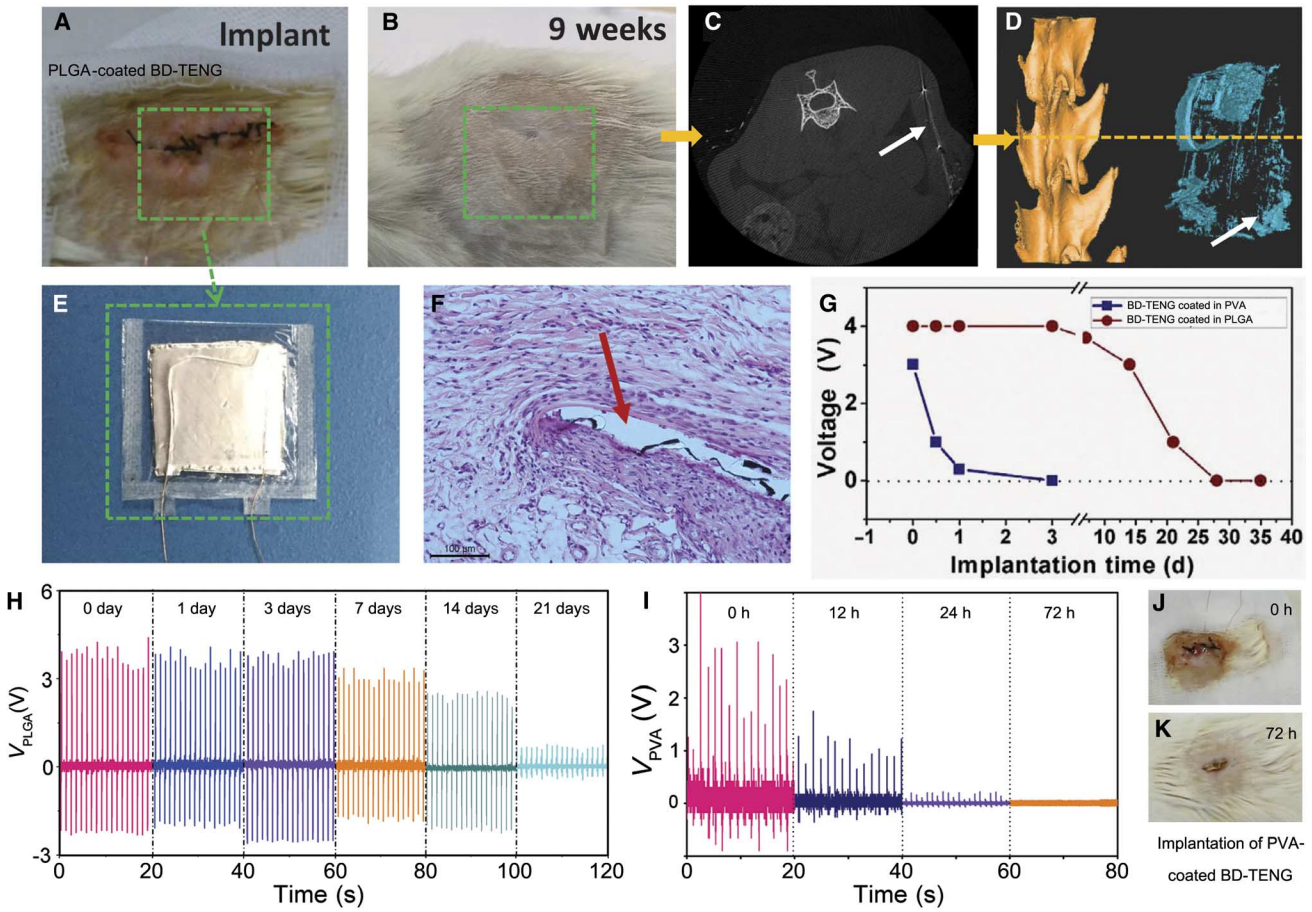

Fig. 4. In vivo biodegradation of BD-TENG. (**A** and **B**) Images of an implanted demonstration for BD-TENG located in the subdermal dorsal region of an SD rat. (A) Implant site right after suture. (B) Implant site after 9 weeks. (**C** and **D**) Micro-CT image of implanted BD-TENG (white arrow) after 9-week implantation demonstrates the degradation degree of BD-TENG in vivo. (C) Cross-section image. (D) Reconstructed three-dimensional image. (**E**) Photograph of BD-TENG before implantation. (**F**) Histological section of tissue at the implant site, excised after 9 weeks, showing a partially resorbed region of the BD-TENG (red arrow). (**G** to **I**) In vivo output of BD-TENGs. (G) Plotted electrical output of BD-TENGs at several time intervals after implantation. (H) Electrical output of BD-TENG that was encapsulated in PLGA. (I) Electrical output of BD-TENG that was encapsulated in PVA. (**J** and **K**) Photograph of implant site of PVA-coated BD-TENG. (J) Right after implantation. (K) Seventy-two hours after implantation.

revealing that water had infiltrated into the encapsulation layer and hydrolyzed the Mg electrodes. Before the rats were executed after 9 weeks of implantation, computed tomography (CT) imaging was carried out. The integrity of the structure had been destroyed, which meant that most materials used for fabricating BD-TENG were biodegraded in the animal body (Fig. 4, C and D).

The PVA-coated BD-TENGs were also evaluated as implantable devices (Fig. 4, J and K). They exhibited an ultratransient degradable property. By applying hydrophobic treatment on the surface, the PVA-coated BD-TENGs could work for over 24 hours in vivo (output, ~3 V) and almost dissolved completely within 72 hours (Fig. 4I).

The application of electric stimulation in tissue engineering provides an exciting route for cell manipulation (*39*). A variety of electrical stimulation techniques have been proven successful in clinical and research settings (*40*–*43*). Here, we combined the BD-TENG with a stimulation device to demonstrate the immediate practicability of using BD-TENG for EF-assisted neuron cell orientation. The stimulation device was composed of two complementary patterned copper electrode networks that were fabricated on a Kapton substrate by high-throughput printing electronics technology. The whole device was covered with a thin polydimethylsiloxane (PDMS) film (100 μm) to avoid the potential electrochemical reaction when copper electrodes were immersed in culture medium (Fig. 5C). Both the spacing between the metal strips and the width of the strips were 100 μm as sketched in Fig. 5D. The BD-TENG with a V_{oc} of 1 V was connected to the electrodes through a rectifying bridge (Fig. 5, A and B). Thus, the EF strength between the two strips was 10 V/mm. However, if considering the thickness of the PDMS coating, the actual amplitude of EF at the cell-device interface was about 7.5 V/cm and was calculated by the finite element method (fig. S6).

Primary neurons were seeded on the stimulation device modified with polylysine and exposed to repeated electrical stimulation after 24-hour culture. EF treatments of 0 (control) and 10 V/mm at 1 Hz were applied for 30 min/day. After 5 days of culturing, the nucleus and cytoskeleton were stained and viewed by laser scanning confocal microscopy (Leica SP8). As shown in Fig. 5, most of the electrically stimulated neurons were well oriented (Fig. 5F). The cytoskeleton of neurons was obviously parallel to the EF, whereas the cell arrangement and cytoskeleton in the control group had no obvious orientation (Fig. 5G and fig. S6).

Cell alignment relative to the EF was further analyzed using National Institutes of Health ImageJ software (version 1.46). The orientation was measured as the angle between 0° and a line drawn through the long axis of the cell with angle values (θ) between 0°and 180°, as shown in Fig. 5H. On the basis of the reported method (*44*), the −cos 2θ was given as a convenient description of cell alignment

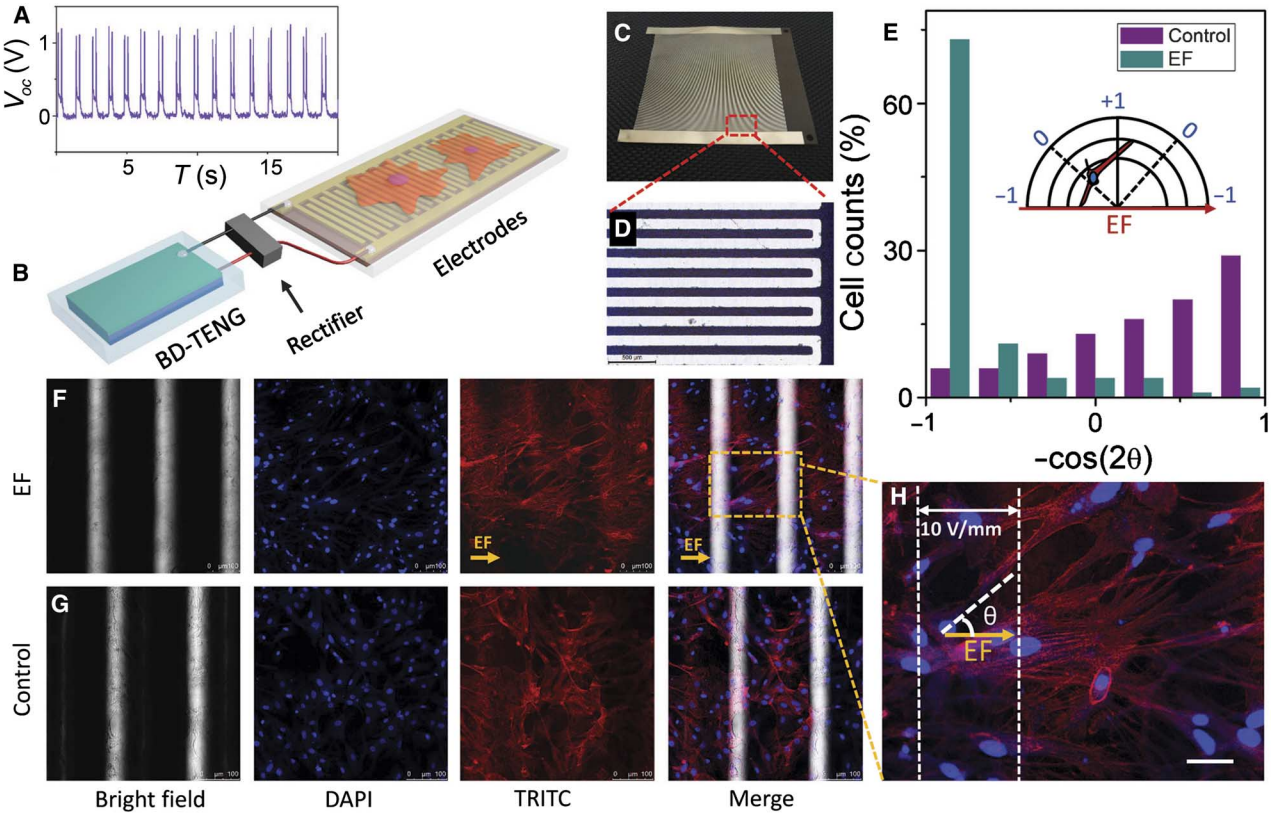

Fig. 5. Electrical stimulation of nerve cells powered by BD-TENG. (**A**) Rectified electrical output of BD-TENG. (**B**) Schematic diagram of self-powered nerve cell stimulation system. (**C**) Photograph of the two complementary patterned electrodes. (**D**) Bright-field microscope image of the electrodes. (**E**) Cell alignment analysis where the cell angle is represented by −cos2θ. (**F** to **H**) Orientation and distribution of nerve cells cultured on the electrodes. (F) Nerve cells with EF stimulation. (G) Nerve cells without EF stimulation. TRITC, tetramethyl rhodamine isothiocyanate. (H) Enlarged view of nerve cells directed by EF (the direction of EF is marked by a yellow arrow; scale bar, 50 μm).

[index of cell alignment (ICA)] where a value near −1 indicates cell alignment parallel to the EF and a value between 0 and +1 indicates random alignment of cells (Fig. 5E). Frequency counts showed that, when simulated with EF, the average value was −0.77, and the 88% of the measured ICAs were distributed between −1 and 0, indicating an obvious tendency of alignment parallel to the EF. However, if without electrical stimulation, the cell angles were randomly distributed between −1 and 1 (Fig. 5E). Neuron cell alignment was significantly directed by the EF from the BD-TENG and was crucial for neural repair.

DISCUSSION

In previous work, EF amplitudes in the order of 0.1 to 10 V/cm have been identified as sufficient to produce an effect without damage, and frequencies <15 Hz are commonly used because aggregates of cells may act as a low-pass filter to the electrical signal (*32*, *45*). At present, noninvasive and implantable electromagnetic devices are used to apply electrical stimulation for tissue repairing. Compared with noninvasive devices, implantable devices ensure patient compliance and treatment efficiency. However, the patients dislike the potential need for additional surgery to remove devices after treatment. The BD-TENG exhibited several distinctive advantages here. When implanted in different sites, it can convert various kinds of biomechanical energy, such as heartbeat, respiratory motion, and the pressure on systolic and diastolic blood vessels, into electrical power. Take the example of the respiratory motion in a rat in which the BD-TENG is implanted under the skin of the left thorax: The inhalation and exhalation of the rat can result in an alternative expansion and contraction of the thorax, which, in turn, produce deformation of the BD-TENG, resulting in the periodical contact and separation between the two fraction layers. In this process, the electric potential induced by the contact electrification and electrostatic induction drives the electrons to flow back and forth through an external circuit in response to the respiratory motion. As the respiratory movement continues, continuous AC output is generated. The considerable biocompatibility and light-weight, cost-effective, and designable size will further facilitate the electric potential's in vivo application. The relatively small amplitudes and the low frequency are just suitable for in vivo electrical stimulation. If integrated with a specially designed electrode or wireless transmission component, fully implantable stimulation or diagnostic devices could be fabricated. Once the therapeutic or diagnostic process is completed, the applied devices can be left behind in the body and will be degraded and absorbed gradually without any residue. These advantages make the BD-TENG an outstanding power source candidate for transient in vivo medical devices.

In summary, we developed a BD-TENG to convert in vivo biomechanical energy into electric power for implantable medical devices. On the basis of a multilayer structure that is composed of BDPs and metals, the BD-TENG produced impressive electrical output power. The combination of the BD-TENG and two complementary micrograting electrodes demonstrated the immediate practicability of using a BD-TENG for EF-assisted neuron cell orientation. Given its in vivo output performance, remarkable biocompatibility, and tunable degradation property, the BD-TENG presented in this work is a potential power source for transient medical devices.

MATERIALS AND METHODS

Fabrication of BD-TENG based on PLGA and PCL

PLGA (75:25, BankVally Ltd.) was dissolved in chloroform at a concentration of 5% (w/v) and cast on a glass plate with a dimension of $D = 6$ cm. The solution was air-dried for 12 hours and then placed in a vacuum oven for another 12 hours to exclude the remaining solvent. Before the film was peeled off, 5 ml of NaOH solution (2 M) was added and reacted for 10 min to create a surface nanostructure. Next, the film was washed with deionized (DI) H_2O three times and dried at 40°C. A patterned PCL (Sigma-Aldrich) film was fabricated in the same process, and the thickness of the as-fabricated films was about 50 to 100 μm. An electrode layer was deposited by the sputtering of magnesium (General Research Institute of Nonferrous Metals, Beijing, China) on the flat side. Then, the two films were fixed together with a spacer set between them, and two lead wires were connected respectively to the electrodes.

A PHV/B (Sigma-Aldrich) film shared the same fabricated process with PLGA and PCL, and the thickness of the as-fabricated films was controlled to 100 μm. PVA (Sigma-Aldrich) is a water-soluble polymer; therefore, it was dissolved in DI H_2O at a concentration of 5% (w/v) and cast on a glass plate.

Encapsulation of BD-TENG

PLGA encapsulation layers were fabricated by the casting method as mentioned above and cut to a proper size. The as-fabricated BD-TENG was set between two PLGA layers. Then, PLGA solution at high concentration (10%, w/v) was used as an adhesive to carefully stick the edge of the two PLGA layers. The device was air-dried for 12 hours and further sealed by a heat sealer to exclude any interstice and ensure that the BD-TENG was protected from the environment. This procedure was also suitable for PVA encapsulation.

Electrical measurements

In vitro test. A liner motor was applied as the external force to drive the BD-TENG (operating distance, 50 mm; maximum speed, 1 m/s; acceleration, 1 m/s^2; deceleration, 1 m/s^2). The resulting applied strain (ε) on the BD-TENG was 0.04%

$$\varepsilon = \frac{h}{2R}$$

where h is the thickness of BD-TENG and R is the bending radius. The V_{oc} was measured by an oscilloscope (Tektronix DPO3034), and the I_{sc} and the transferred charge were detected by an electrometer (Keithley 6517B).

In vivo test. To measure the electrical signal of BD-TENG when it biodegrades in vivo, we implanted the BD-TENG in the subdermal region of the backs of SD rats where observation is much easier. Moreover, this implant region can facilitate our subsequent measurements and avoid the lead wires being destroyed by rats' scratching. To effectively drive the implanted BD-TENG and evaluate its output property at different time points in vivo, we applied an external force

by a slight finger tap on the skin of the implanted region. The as-generated output signals were measured by connecting the lead wires to electrodes of the oscilloscope or the electrometer.

Primary culture of SD neonatal rat nerve cells

The cerebral cortex of an SD neonatal rat was processed to separate and purify nerve cells by mechanical trituration, trypsinization (0.1% trypsin digestion), filtration, and centrifugation. Trypan blue staining showed that 79.8% of primary cultured nerve cells were positive. The purified cells were cultured in Dulbecco's modified Eagle's medium (Hyclone) containing 10% fetal bovin serum (Gibco) and 1% penicillin-streptomycin solution (Macgene). Nerve cells were seeded at a density of 30,000 cells/cm^2 on the interdigital electrodes and incubated at 37°C in a humidified atmosphere with 5% CO_2.

Electric stimulation powered by the TENG

After 24 hours in culture, the nerve cells were exposed to DC electric treatment of about 1 V, which was transformed from the AC output of BD-TENG by a Schottky bridge rectifier (MB12S; Micro Commercial Components). The theoretical value of the DC-EF between the two strips of the stimulation device was about 10 V/mm. If considering the thickness of the PDMS (SYLGARD 184, Dow Corning) coating (100 μm), the actual amplitude of EF at the surface was about 7.5 V/cm. This DC-EF (1 Hz) was applied to neuronal cells for 20 min/day for 5 days.

Cell morphology and immunofluorescence staining

On day 6, the cytoskeleton and nucleus were stained with phalloidin and 4′,6-diamidino-2-phenylindole (DAPI), respectively. Samples were fixed with immunohistochemically fixed fluid (Beyotime) for 15 min and rinsed three times with prewarmed PBS. Samples were blocked with 0.1% bovine serum albumin solution for 1 hour at 37°C and then incubated with DAPI (1:400 dilution) and Alexa Fluor 568–phalloidin conjugate (1:200 dilution) for 2 hours at 37°C. Nerve cells were imaged using laser scanning confocal microscopy (*46*).

SUPPLEMENTARY MATERIALS

Supplementary material for this article is available at http://advances.sciencemag.org/cgi/content/full/2/3/e1501478/DC1

Fig. S1. Typical output performance of BD-TENG.

Fig. S2. In vitro degradation of BDPs and metal electrode.

Fig. S3. Water contact angle test of selected BDPs.

Fig. S4. Bright-field microscope image of tissue fluid smears without any stain.

Fig. S5. Calculated distribution of the EF of the stimulation device via finite element method (assuming that the input voltage of BD-TENG was 1 V).

Fig. S6. A larger view of nerve cells cultured on the electrodes.

REFERENCES AND NOTES

1. M. Irimia-Vladu, "Green" electronics: Biodegradable and biocompatible materials and devices for sustainable future. *Chem. Soc. Rev.* **43**, 588–610 (2014)
2. J. A. Rogers, Electronics for the human body. *JAMA* **313**, 561–562 (2015).
3. K. Bazaka, M. V. Jacob, Implantable devices: Issues and challenges. *Electronics* **2**, 1–34 (2013).
4. B. Tian, X. Zheng, T. J. Kempa, Y. Fang, N. Yu, G. Yu, J. Huang, C. M. Lieber, Coaxial silicon nanowires as solar cells and nanoelectronic power sources. *Nature* **449**, 885–889 (2007).
5. C. J. Bettinger, Z. Bao, Organic thin-film transistors fabricated on resorbable biomaterial substrates. *Adv. Mater.* **22**, 651–655 (2010).
6. M. Irimia-Vladu, P. A. Troshin, M. Reisinger, L. Shmygleva, Y. Kanbur, G. Schwabegger, M. Bodea, R. Schwödiauer, A. Mumyatov, J. W. Fergus, V. F. Razumov, H. Sitter, N. S. Sariciftci, S. Bauer, Biocompatible and biodegradable materials for organic field-effect transistors. *Adv. Funct. Mater.* **20**, 4069–4076 (2010).
7. D.-H. Kim, N. Lu, R. Ma, Y.-S. Kim, R.-H. Kim, S. Wang, J. Wu, S. M. Won, H. Tao, A. Islam, K. J. Yu, T.-. Kim, R. Chowdhury, M. Ying, L. Xu, M. Li, H.-J. Chung, H. Keum, M. McCormick, P. Liu, Y.-W. Zhang, F. G. Omenetto, Y. Huang, T. Coleman, J. A. Rogers, Epidermal electronics. *Science* **333**, 838–843 (2011).
8. F. G. Omenetto, D. L. Kaplan, New opportunities for an ancient material. *Science* **329**, 528–531 (2010).
9. Z. Li, G. Zhu, R. Yang, A. C. Wang, Z. L. Wang, Muscle-driven in vivo nanogenerator. *Adv. Mater.* **22**, 2534–2537 (2010).
10. S.-W. Hwang, H. Tao, D.-H. Kim, H. Cheng, J.-K. Song, E. Rill, M. A. Brenckle, B. Panilaitis, S. M. Won, Y.-S. Kim, Y. M. Song, K. J. Yu, A. Ameen, R. Li, Y. Su, M. Yang, D. L. Kaplan, M. R. Zakin, M. J. Slepian, Y. Huang, F. G. Omenetto, J. A. Rogers, A physically transient form of silicon electronics. *Science* **337**, 1640–1644 (2012).
11. D.-H. Kim, J. Viventi, J. J. Amsden, J. Xiao, L. Vigeland, Y.-S. Kim, J. A. Blanco, B. Panilaitis, E. S. Frechette, D. Contreras, D. L. Kaplan, F. G. Omenetto, Y. Huang, K.-C. Hwang, M. R. Zakin, B. Litt, J. A. Rogers, Dissolvable films of silk fibroin for ultrathin conformal bio-integrated electronics. *Nat. Mater.* **9**, 511–517 (2010).
12. F. Patolsky, C. M. Lieber, Nanowire nanosensors. *Mater. Today* **8**, 20–28 (2005).
13. C.-H. Wang, C.-Y. Hsieh, J.-C. Hwang, Flexible organic thin-film transistors with silk fibroin as the gate dielectric. *Adv. Mater.* **23**, 1630–1634 (2011).
14. M. Irimia-Vladu, P. A. Troshin, M. Reisinger, G. Schwabegger, M. Ullah, R. Schwoediauer, A. Mumyatov, M. Bodea, J. W. Fergus, V. F. Razumov, H. Sitter, S. Bauer, N. S. Sariciftci, Environmentally sustainable organic field effect transistors. *Org. Electron.* **11**, 1974–1990 (2010).
15. S.-W. Hwang, J.-K. Song, X. Huang, H. Cheng, S.-K. Kang, B. H. Kim, J.-H. Kim, S. Yu, Y. Huang, J. A. Rogers, High-performance biodegradable/transient electronics on biodegradable polymers. *Adv. Mater.* **26**, 3905–3911 (2014).
16. S.-W. Hwang, C. H. Lee, H. Cheng, J.-W. Jeong, S.-K. Kang,J.-H. Kim, J. Shin, J. Yang, Z. Liu, G. A. Ameer, Y. Huang, J. A. Rogers, Biodegradable elastomers and silicon nanomembranes/nanoribbons for stretchable, transient electronics, and biosensors. *Nano Lett.* **15**, 2801–2808 (2015).
17. C. Dagdeviren, S.-W. Hwang, Y. Su, S. Kim, H. Cheng, O. Gur, R. Haney, F. G. Omenetto, Y. Huang, J. A. Rogers, Transient, biocompatible electronics and energy harvesters based on ZnO. *Small* **9**, 3398–3404 (2013).
18. M. A. Hannan, S. Mutashar, S. A. Samad, A. Hussain, Energy harvesting for the implantable biomedical devices: Issues and challenges. *Biomed. Eng. Online* **13**, 79 (2014).
19. R. A. Gross, B. Kalra, Biodegradable polymers for the environment. *Science* **297**, 803–807 (2002).
20. A. C. Fonseca, M. H. Gil, P. N. Simões, Biodegradable poly(ester amide)s—A remarkable opportunity for the biomedical area: Review on the synthesis, characterization and applications. *Prog. Polym. Sci.* **39**, 1291–1311 (2014).
21. Z. L. Wang, Triboelectric nanogenerators as new energy technology for self-powered systems and as active mechanical and chemical sensors. *ACS Nano* **7**, 9533–9557 (2013).
22. Z. L. Wang, J. Chen, L. Lin, Progress in triboelectric nanogenerators as a new energy technology and self-powered sensors. *Energ. Environ. Sci.* **8**, 2250–2282 (2015).
23. Z.-H. Lin, G. Cheng, L. Lin, S. Lee, Z. L. Wang, Water-solid surface contact electrification and its use for harvesting liquid-wave energy. *Angew. Chem. Int. Ed. Engl.* **52**, 12545–12549 (2013).
24. J. Chen, G. Zhu, W. Yang, Q. Jing, P. Bai, Y. Yang, T.-C. Hou, Z. L. Wang, Harmonic-resonator-based triboelectric nanogenerator as a sustainable power source and a self-powered active vibration sensor. *Adv. Mater.* **25**, 6094–6099 (2013).
25. Q. Zheng, B. Shi, F. Fan, X. Wang, L. Yan, W. Yuan, S. Wang, H. Liu, Z. Li, Z. L. Wang, In vivo powering of pacemaker by breathing-driven implanted triboelectric nanogenerator. *Adv. Mater.* **26**, 5851–5856 (2014).
26. S. Wang, L. Lin, Z. L. Wang, Triboelectric nanogenerators as self-powered active sensors. *Nano Energy* **11**, 436–462 (2015).
27. X.-S. Zhang, M.-D. Han, R.-X. Wang, F.-Y. Zhu, Z.-H. Li, W. Wang, H.-X. Zhang, Frequency-multiplication high-output triboelectric nanogenerator for sustainably powering biomedical microsystems. *Nano Lett.* **13**, 1168–1172 (2013).
28. C. Zhang, W. Tang, C. Han, F. Fan, Z. L. Wang, Theoretical comparison, equivalent transformation, and conjunction operations of electromagnetic induction generator and triboelectric nanogenerator for harvesting mechanical energy. *Adv. Mater.* **26**, 3580–3591 (2014).
29. F.-R. Fan, L. Lin, G. Zhu, W. Wu, R. Zhang, Z. L. Wang, Transparent triboelectric nanogenerators and self-powered pressure sensors based on micropatterned plastic films. *Nano Lett.* **12**, 3109–3114 (2012).
30. G. Zhu, C. Pan, W. Guo, C.-Y. Chen, Y. Zhou, R. Yu, Z. L. Wang, Triboelectric-generator-driven pulse electrodeposition for micropatterning. *Nano Lett.* **12**, 4960–4965 (2012).
31. C. K. Jeong, K. M. Baek, S. Niu, T. W. Nam, Y. H. Hur, D. Y. Park, G.-T. Hwang, M. Byun, Z. L. Wang, Y. S. Jung, K. J. Lee, Topographically-designed triboelectric nanogenerator via block copolymer self-assembly. *Nano Lett.* **14**, 7031–7038, (2014).

32. S. D. McCullen, J. P. McQuilling, R. M. Grossfeld, J. L. Lubischer, L. I. Clarke, E. G. Loboa, Application of low-frequency alternating current electric fields via interdigitated electrodes: Effects on cellular viability, cytoplasmic calcium, and osteogenic differentiation of human adipose-derived stem cells. *Tissue Eng. Part C Methods* **16**, 1377–1386 (2010).
33. N. Lucas, C. Bienaime, C. Belloy, M. Queneudec, F. Silvestre, J.-E. Nava-Saucedo, Polymer biodegradation: Mechanisms and estimation techniques. *Chemosphere* **73**, 429–442 (2008).
34. K. Leja, G. Lewandowicz, Polymer biodegradation and biodegradable polymers-–A review. *Polish J. of Environ. Stud.* **19**, 255–266 (2010).
35. B. M. Holzapfel, J. C. Reichert, J.-T. Schantz, U. Gbureck, L. Rackwitz, U. Nöth, F. Jakob, M. Rudert, J. Groll, D. W. Hutmacher, How smart do biomaterials need to be? A translational science and clinical point of view. *Adv. Drug Deliver. Rev.* **65**, 581–603 (2013).
36. T. Freier, C. Kunze, C. Nischan, S. Kramer, K. Sternberg, M. Saß, U. T. Hopt, K.-P. Schmitz, In vitro and in vivo degradation studies for development of a biodegradable patch based on poly(3-hydroxybutyrate). *Biomaterials* **23**, 2649–2657 (2002).
37. M. A. Woodruff, D. W. Hutmacher, The return of a forgotten polymer—Polycaprolactone in the 21st century. *Prog. Polym. Sci.* **35**, 1217–1256 (2010).
38. M. Abedalwafa, F. Wang, L. Wang, C. Li, Biodegradable poly-epsilon-caprolactone (Pcl) for tissue engineering applications: A review. *Rev. Adv. Mater. Sci.* **34**, 123–140 (2013).
39. S. Meng, M. Rouabhia, Z. Zhang, Electrical stimulation in tissue regeneration, in *Applied Biomedical Engineering*, G. Gargiulo, Ed. (InTech, Rijeka, Croatia, 2011).
40. D. M. Ciombor, R. K. Aaron, The role of electrical stimulation in bone repair. *Foot Ankle Clin.* **10**, 579–593 (2005).
41. M. Zhao, B. Song, J. Pu, T. Wada, B. Reid, G. Tai, F. Wang, A. Guo, P. Walczysko, Y. Gu, T. Sasaki, A. Suzuki, J. V. Forrester, H. R. Bourne, P. N. Devreotes, C. D. McCaig, J. M. Penninger, Electrical signals control wound healing through phosphatidylinositol-3-OH kinase-γ and PTEN. *Nature* **442**, 457–460 (2006).
42. J. C. Gan, P. A. Glazer, Electrical stimulation therapies for spinal fusions: Current concepts. *Eur. Spine J.* **15**, 1301–1311 (2006).
43. C. T. Brighton, S. R. Pollack, Treatment of recalcitrant non-union with a capacitively coupled electrical-field. A preliminary report. *J. Bone Joint Surg. Am.* **67**, 577–585 (1985).
44. H. T. Nguyen, C. Wei, J. K. Chow, L. Nguy, H. K. Nguyen, C. E. Schmidt, Electric field stimulation through a substrate influences Schwann cell and extracellular matrix structure. *J. Neural Eng.* **10**, 046011 (2013).
45. L. Li, Y. H. El-Hayek, B. Liu, Y. Chen, E. Gomez, X. Wu, K. Ning, L. Li, N. Chang, L. Zhang, Z. Wang, X. Hu, Q. Wan, Direct-current electrical field guides neuronal stem/progenitor cell migration. *Stem Cells* **26**, 2193–2200 (2008).
46. W. Seung, M. K. Gupta, K. Y. Lee, K.-S. Shin, J.-H. Lee, T. Y. Kim, S. Kim, J. Lin, J. H. Kim, S.-W. Kim, Nanopatterned textile-based wearable triboelectric nanogenerator. *ACS Nano* **9**, 3501–3509 (2015).

Acknowledgments: We thank H. Liu for his suggestion in data processing and L. Yan for assistance in three-dimensional figure preparation. **Funding:** This work was supported by the Thousands Talents program for pioneer researcher (Z.L.W.) and his innovation team, National Science Foundation of China (31200702 and 31571006), and Beijing Nova Program (Z121103002512019). **Author contributions:** Z.L.W. and Z. Li designed the research; Q.Z. and Y. Zou fabricated the devices and implemented the in vitro and in vivo tests; Y. Zou, Y. Zhang, and Z. Liu assisted in designing the device structure and performing cell experiments; B.S. assisted in electrical measurements; X.W., Y.J., and H.O. contributed analytical tools; and Q.Z., Z.L.W., and Z. Li wrote the paper. All authors contributed to the discussion of the results and approved the final version. **Competing interests:** The authors declare that they have no competing interests. **Data and materials availability:** All data needed to evaluate the conclusions in the paper are present in the paper and/or the Supplementary Materials. Additional data related to this paper may be requested from the authors.

Submitted 17 October 2015
Accepted 5 January 2016
Published 4 March 2016
10.1126/sciadv.1501478

Citation: Q. Zheng, Y. Zou, Y. Zhang, Z. Liu, B. Shi, X. Wang, Y. Jin, H. Ouyang, Z. Li, Z. L. Wang, Biodegradable triboelectric nanogenerator as a life-time designed implantable power source. *Sci. Adv.* **2**, e1501478 (2016).

ScienceAdvances
AAAS

Biodegradable triboelectric nanogenerator as a life-time designed implantable power source

Qiang Zheng, Yang Zou, Yalan Zhang, Zhuo Liu, Bojing Shi, Xinxin Wang, Yiming Jin, Han Ouyang, Zhou Li and Zhong Lin Wang (March 4, 2016)

Sci Adv 2016, 2:.
doi: 10.1126/sciadv.1501478